Field tests of a highly flexible downwind ultralight rotor to mimic a 13-MW turbine rotor

Eric Loth [1], Gavin Ananda [2], Mayank Chetan [3], Rick Damiani [4], D. Todd Griffith [3], Kathryn Johnson [5], Sepideh Kianbakht [5], Meghan Kaminski [1], Lucy Pao [6], Mandar Phadnis [6], Chao (Chris) Qin [1], Andy Scholbrock [7], Michael Selig [2], Juliet Simpson [1] and Shulong Yao [3]

[1] *Department of Mechanical and Aerospace Engineering, University of Virginia*
[2] *Department of Aerospace Engineering, University of Illinois at Urbana-Champaign*
[3] *Department of Mechanical Engineering, University of Texas at Dallas*
[4] *RRD Engineering, LLC*
[5] *Department of Electrical Engineering, Colorado School of Mines*
[6] *Department of Electrical, Computer, and Energy Engineering, University of Colorado Boulder*
[7] *National Wind Technology Center, National Renewable Energy Laboratory*

E-mail: loth@virginia.edu

Keywords: downwind, extreme-scale, flexible, rotor

Abstract. Offshore extreme-scale turbines of 20–25 MW in size may offer reduced energy costs. The technical barriers at these extreme scales include escalating blade masses with increased flexibility as well as high gravity loads and tower-strike issues. These barriers may be addressed with a load-aligning downwind turbine. To investigate this type of design, a field test campaign was conducted with an aeroelastically scaled rotor, termed the Segmented Ultralight Morphing Rotor Demonstrator (SUMR-D). The tests were conducted on the Controls Advanced Research Turbine at the National Renewable Energy Laboratory. The paper gives an overviewof the experimental diagnostics, blade design, and results of the field campaign, as well as makes conclusions and recommendations regarding extreme-scale highly flexible downwind rotors.

1. Introduction: Downwind load-aligning rotor

As turbine sizes increase to reduce cost, the aerodynamic and mass loads on the blades increase quickly. As shown in figure 1a, the rated loads on an upwind rotor blade include a combination of centrifugal, cantilever, and thrust forces. This average downwind load-path angle increases as the turbine size grows, e.g., the load-path angle is less than 10° for 5-MW turbines but more than 20° for 16-MW turbines [1, 2]. This leads to increased structural mass to resist these flapwise moments and to meet clearance requirements necessary to prevent tower strike. The Segmented Ultralight Morphing Rotor (SUMR)

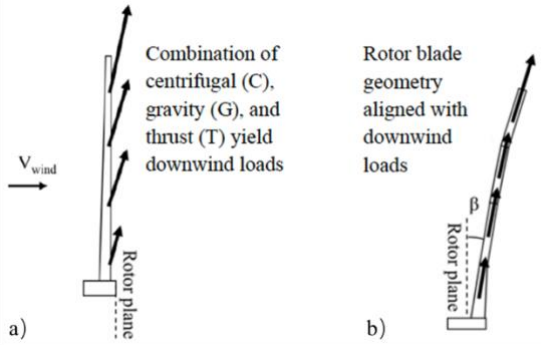

Figure 1. Side-view of non-torque rotor forces for: a) a conventional upwind blade and b) a downwind load-aligned blade.

concept uses a downwind rotor with load-aligning coning and aeroelastic deflecting blades, as shown in figure 1b, to reduce flapwise blade moments and to make the tower-strike clearance less problematic. For 13-MW and 25-MW turbines, the net effect is a reduced rotor mass compared to a conventional upwind rotor [3–5]. Reducing flapwise moment also makes blade segmentation more feasible since the loads at the joints can be reduced. Furthermore, wake losses are reduced with a downwind design because the shaft tilt angle can be angled to promote a downward shift of the wake and entrainment of higher momentum air from above. This increased entrainment can also make wake steering more efficient. As such, a highly flexible downwind load-aligned design at extreme scales has four key potential advantages:

1. Reduced flapwise moments and tower strike probability
2. Reduced rotor mass (due to above aspects)
3. Facilitated use of blade segmentation
4. Reduced wake losses for downwind turbines

Given these benefits, there is a growing interest in downwind turbines. A recent project on SUMR turbines employed a computational design approach that quantified the first two advantages for a 13.2-MW turbine (SUMR-13) and a 25-MW turbine (SUMR-25) relative to conventional upwind turbines. Work is ongoing to quantify the last two advantages for a 25-MW design. However, turbine designers have noted four key critical concerns for downwind turbines:

1. Increased complexity associated with flexible lighter blades
2. Increased noise in the form of a low-frequency “thumping” noise
3. Increased fatigue due to tower shadow
4. Reduced power due to a potentially reduced swept area

The SUMR field test campaign was designed to mimic the aeroelastic performance of a highly coned 13-MW downwind design and provide experimental evidence that can support the first two advantages and can help evaluate all four of the concerns. This subscale turbine rotor was designed to produce nearly the same load angles for both steady conditions (figure 1) of a 13.2-MW turbine as well as nearly the same load angle fluctuations for unsteady conditions due to turbulence, aeroelastic response, and rotor dynamics and control. This is the first downwind turbine field test to employ such scaling.

The following section highlights the scaling approach used for the demonstrator rotor (Section 2), followed by aerodynamic design and structural design (Sections 3 and 4), installation, operations, and test methods (Sections 5 and 6), controller performance for operation and for shutdown (Sections 7 and 8), as well as blade loads and tower shadow (Section 9).

2. Gravo-aeroelastic scaling of the rotor

To evaluate the advantages and concerns associated with downwind turbines, a field test campaign was conducted with the Segmented Ultralight Morphing Rotor Demonstrator (SUMR-D) mounted on the two-bladed Controls Advanced Research Turbine (CART2) at the National Renewable Energy Laboratory’s (NREL’s) Flatirons Campus (figure 2). The experimental demonstrator test turbine (SUMR-D) was a scaled-down version of a SUMR-13 turbine designed for Class IIB wind speeds with a 50-year gust of 59.5 m/s and a turbulence intensity of 14%. The aeroelastic scaling aimed to replicate the nondimensional (mean and unsteady) blade

Figure 2. SUMR rotor on CART2 with 12.5° coning (credit NREL)

deflections and flapwise moments of the full-scale system as a function of wind speed normalized by the rated speed [6–10].

Figure 3 shows the nondimensional blade stiffness distribution of the as-built SUMR-D compared to the ideal SUMR-13 turbine. Higher stiffness was employed at the root to include an adapter to connect to the CART2. The outboard section had mass distributions consistent with the scaled values, which is critical for matching full-scale dynamics. However, some additional stiffness was needed due to test system requirements for the NREL Flatirons Campus, which can exhibit extreme winds (>45 m/s).

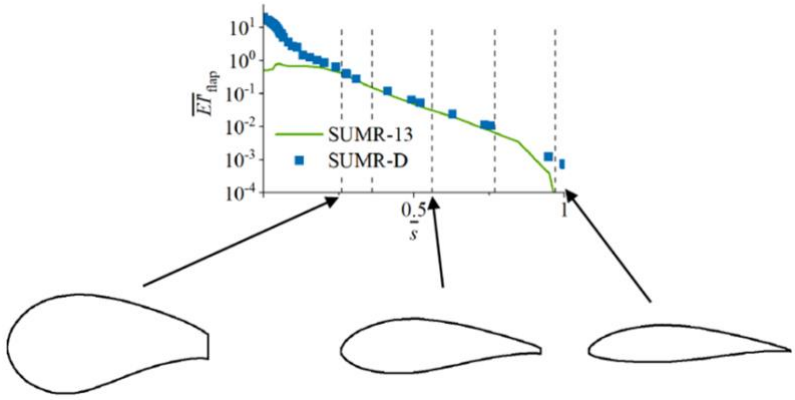

Figure 3. Nondimensional blade sectional stiffness vs. nondimensional span of SUMR-13 and as-built SUMR-D along with sample airfoil shapes at 26%, 56%, and 97% span.

3. Aerodynamic design of SUMR-13 and SUMR-D

The rotor and the airfoil sections of the SUMR-13 were designed separately using an inverse design approach in which the desired aerodynamic performance parameters were prescribed, and the geometry that would yield that performance was obtained. The two design tools used for blade and airfoil designs were PROPID [11, 12] and PROFOIL [13, 14], per figure 4.

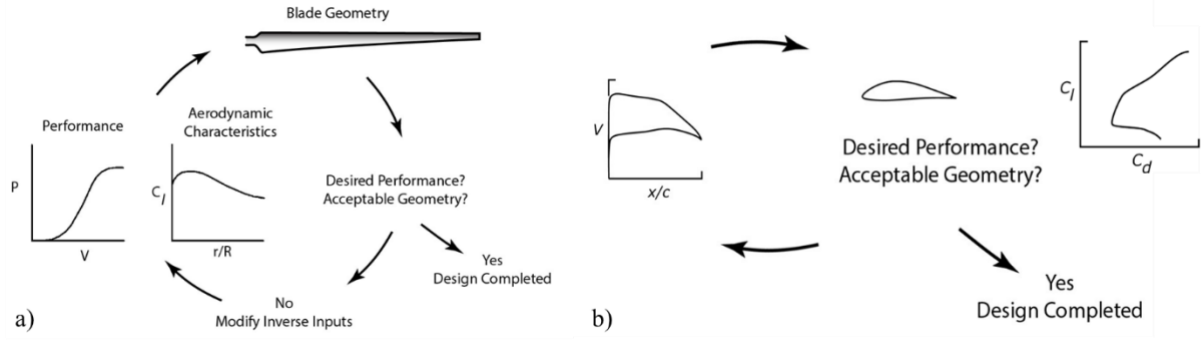

Figure 4. Inverse design tools: a) PROPID for rotor design and b) PROFOIL for airfoil design.

In PROPID, the desired performance from the rotor is specified via prescription of the rated power, operating tip-speed ratio, average and rated wind speeds, axial induction distribution along the blade length, and the C_L (lift coefficient) distribution along the blade length, usually corresponding to the highest lift-to-drag ratio (L/D) of each of the airfoil cross sections. Based on the aforementioned design parameters, the rotor geometry is obtained in terms of rotor diameter, blade pitch, and blade chord and twist distributions. PROFOIL is an inverse airfoil design tool that allows for the prescription of the appropriate airfoil velocity distributions that yield, via the inverse methodology, the corresponding airfoil geometry. The airfoil geometry is then analyzed in XFOIL [15, 16], and based on the desired performance, the velocity profiles are adjusted again. The process is iterated to converge to an optimum airfoil design.

For the SUMR-13 design [17], an initial blade thickness distribution was set based on historical precedence and input from the structures team. New airfoils were designed using PROFOIL by

maximizing L/D at specific operating design lift coefficients. Based on the expected size of the rotor radius, R, to produce a rated power of 13.2 MW (R = 100 m), the operating tip-speed ratio (TSR = 9.5), and the average and rated wind speeds (V_{avg} = 8.5 m/s, V_{rated} = 11.3 m/s), the chordwise Reynolds numbers varied from 4×10^6 near the hub to 15×10^6 near the tip. At these high Reynolds numbers and blade thicknesses that supported structural optimization, the high-performance F1-series of flatback and sharp trailing-edge airfoils were designed in PROFOIL. Following that, the blade pitch, radius, and chord and twist distribution were designed using PROPID. The aerodynamic performance data were then confirmed with OpenFAST, NREL's aero-hydro-servo-elastic code [18]. With the aerodynamic design completed, a few iterations were carried out between the controls and structural design teams with a threefold objective. The first goal was to maximize power output at the average and rated wind speeds specified [19, 20]. The second objective was to ensure that predicted structural loads were within allowable limits following the International Electrotechnical Commission (IEC) [21] standards. The third objective was to minimize rotor mass, therefore demonstrating a reduction in rotor costs via the SUMR configuration.

The SUMR-D blade was geometrically scaled from the SUMR-13 to a blade length of 20.87 m. No changes to the airfoil shape or planform were made. As such, the aerodynamic efficiency of the SUMR-D is lower than the SUMR-13 because the airfoils operate at suboptimal Reynolds numbers (deemed acceptable as the power coefficients are not a focus of the SUMR-D test campaign).

4. SUMR-D structural design

An important question toward the realization of larger rotor designs is how to configure and optimize structural designs to constrain blade mass and cost while meeting a growing set of challenging structural design requirements. Earlier studies completed detailed structural design of rotors at the 13.2-MW scale that are upwind [22] and downwind [23]. The downwind rotor was predicted to achieve 25% rotor mass reduction [23] compared to the upwind rotor [22]. However, field testing was warranted to experimentally demonstrate the performance of this downwind, highly coned design. The SUMR-D structural design [7, 10] was based on two competing objectives: gravo-aeroelastic scaling, which yields an ultralight design and site-specific structural safety criteria that tend to increase blade weight (table 1). As detailed [7], these competing objectives were met, including a good agreement for nondimensional tip deflection and flapwise blade frequency (both within 2.1%) with accurate blade mass distribution while meeting strict strength requirements for a testing site that can experience up to 45 m/s wind gusts. A sample design cross section is shown in figure 5. The as-built blade had additional mass due to fabrication, which further reduced frequency and flexibility (table 1).

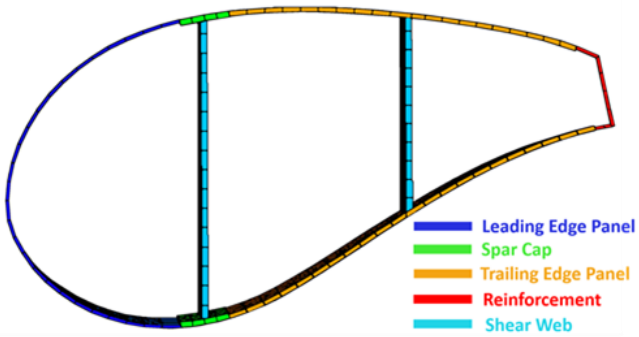

Figure 5. SUMR-D structural design at max chord.

In order to gain an additional understanding of the SUMR-D structural performance, a multi-fidelity digital twin structural model (virtual model) was developed for the SUMR-D as-built design [24]. The goal was to develop and demonstrate an approach to produce an accurate and detailed model of the as-built blade for use in verifying the performance of the operating two-bladed, downwind rotor. This method follows the rotor from the stages of design to manufacturing, then to the ground testing and field operation. The result is an accurate multi-fidelity digital twin model for the geometric, structural, and structural dynamic properties of the as-built blade within a 1% match in mass properties, 3.2% in blade frequencies, and 6% in deflection [24].

Table 1. Summary of the SUMR-D gravo-aeroelastic scaling target, design, and digital twins.

	GAS Target	Design	As Built
Blade mass [kg]	351	827	995
Center of gravity [m]	-	4.6	4.94
1st flapwise frequency at rated [Hz]	1.53	1.5	1.22
Nondimensional flapwise frequency [-]	4.18	4.10	3.33
Tip deflection [m]	1.42	1.39	1.18
Nondimensional tip deflection [-]	0.068	0.067	0.056

5. SUMR-D field test and installation constraints

Several design and operational considerations had to be implemented to allow for the gravo-aeroelastically scaled rotor of the SUMR turbine to be tested on the CART2.

First, a dedicated aero-servo-elastic load analysis was carried out to account for actual conditions to be expected at NREL's Flatirons Campus. The results in terms of ultimate limit states with appropriate partial safety factors [9] were used to both guide the blade structural design (above) and to verify the structural and mechanical viability of mounting the SUMR-D rotor onto the CART2. Meeting the requirements for the high loads that could be encountered under extreme and fault conditions at the test site and accounting for accumulating fatigue damage throughout the period of deployment required using more layers (overlaminates) of composite materials than originally devised (figure 5). Additionally, the aggressive aerodynamic twist profile of the blade required that the outer mold line be specially clocked with bond lines adjusted and "glue-lips" and removable flanges devised to prevent "draft-locking" in the molds. Finally, a blade tip, not included in either the aerodynamic or structural design, was adapted to the last defined airfoil and manufactured to cap the blade smoothly. One of the two blades with its mounting adapter was subjected to both a proof load and a modal test on a test stand. The tests verified both the predicted strength and eigenfrequencies of the manufactured blade.

Second, the CART2 had to be reconfigured to run in downwind mode, which triggered several actions. To maintain the usual clockwise rotation direction of the drivetrain, the blade camber was reversed to a left-hand profile. Further, the turbine yaw control system and the nacelle wind vane were reset to operate with a 180° offset. The pitch system also had to be reversed in direction, thus swapping the conventional pitch settings for "run" and "feather."

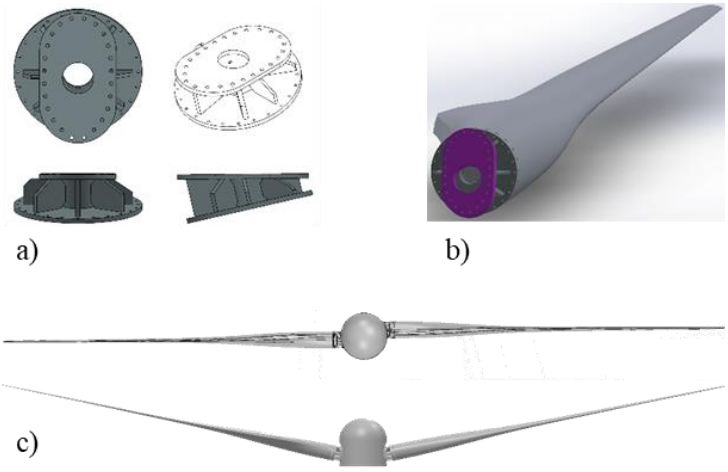

Figure 6. Views of a) the mounting adapter for pre-coning, b) the blade connected to the spindle plate, and c) the rotor downwind rotor view for feathered and above view for run.

Third, to create the 12.5° coning of the rotor, a special blade adapter was designed and manufactured out of steel (figure 6). The adapter was verified via a dedicated finite-element analysis [9] under the extreme loads that had already been calculated for the blade root. Because the pitch axis lies at the coning angle from the blade axis, the blade describes a conical surface when pitching, and in the feathered configuration, the axes of the two blades do not intersect (figure 6c). As a consequence, there is an additional pitching torque since the blade's center of mass is offset from the pitch axis and the

blade aerodynamic loading. Based on the loads calculated in the aero-servo-elastic simulations, the pitch drive was able to resist the applied torque.

Fourth, due to the absence of a rotor lock and the CART2's mechanical brake capacity, the rotor and hub assembly had to be lowered to allow for the ground installation of the SUMR-D blades. On the ground, both the hub and spindles had to be independently rotated about their respective axes to mount the new blades. In the final lift to the nacelle, the blades were (unconventionally) pitched to run so that they would lie on the same horizontal plane with equal length lifting slings attached to a spreader bar.

6. Demonstrator operations and test methods

To operate the CART2 wind turbine with the SUMR-D rotor, several modifications needed to be made to the turbine and its custom-built 400-Hz synchronous control and data-acquisition system. First, since this research turbine is primarily used in its upwind configuration, sensors needed to be adjusted in order to allow the turbine to run in a downwind configuration. For instance, the nacelle wind vane needed to be turned 180° from its original mounting configuration such that its dead band was outside of the new normal downwind operating configuration. The absolute yaw encoder had to be adjusted by applying an offset of an additional 180° to its original calibrated value such that a true north reading is when the rotor is due south of the tower. Strain gauge orientations had to be changed and new calibrations applied because of the new configuration, and cameras and blade targets were added to sense blade deflection. Since the turbine's gearbox is designed to operate in one direction, the turbine rotated in the same fashion as in its upwind configuration, i.e., counterclockwise for an observer standing upwind of the turbine. With this, the sensors for torque and rotational speed did not need to be adjusted.

During commissioning, it was found that the blades began to oscillate within the first 10 seconds of startup. Upon reviewing the data in figure 7, it became evident that the pitch controller was driving an oscillation in the highly flexible blades, which was then inducing an oscillation in the drivetrain. The oscillation in the high-speed shaft was then fed back into the pitch controller, which caused a positive feedback loop that grew in an undamped fashion. After evaluating the frequency of the combined blade pitch-drivetrain instability, a second-order low-pass filter was applied to the pitch controller, resulting in nominal operation of the wind turbine for the remainder of the data collection period for the SUMR-D field experiment on the CART2 wind turbine. Notably, this instability was not captured during

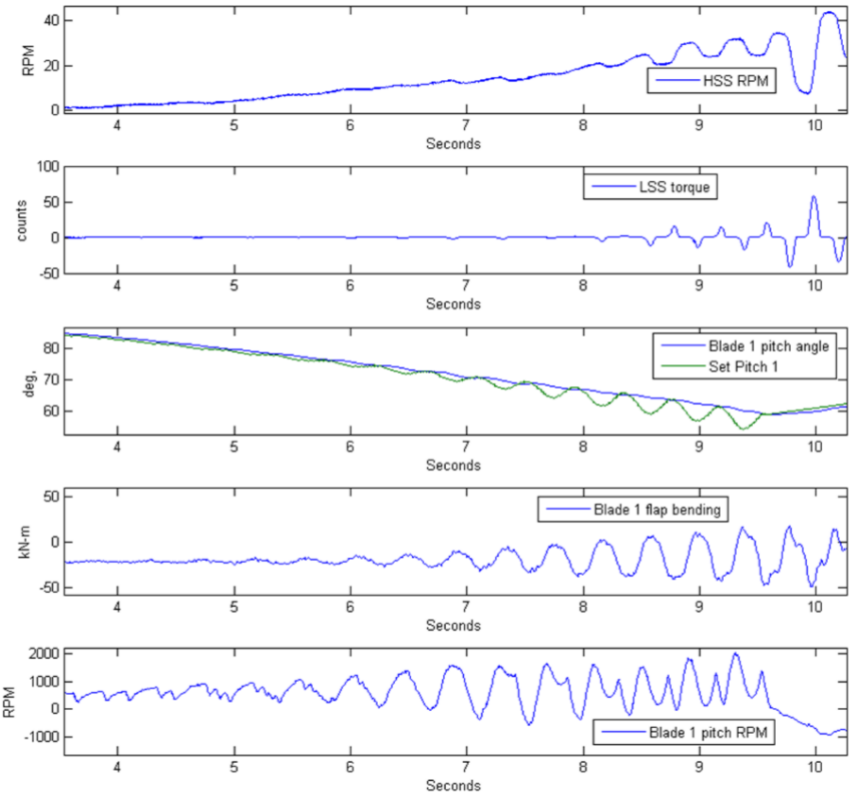

Figure 7. CART data showing coupling of the blade pitch with the first flap mode of the blades and the turbine's drivetrain.

the modeling and simulation effort ahead of the field experiment. Thus, it is clear that research of this nature greatly benefits from an in situ field experiment.

7. SUMR-D simulated aerodynamic flow field and operational controller

For an accurate comparison, it was important to recreate the field conditions in the simulations as closely as possible. The available field sensors for measuring wind speeds included a cup anemometer at hub height on the turbine nacelle as well as anemometers on a meteorological (met) mast that was 40 m upstream of the turbine. The met mast sensors consisted of a sonic anemometer at hub height that measured wind in the downwind *u* and transverse *v* and *w* directions and met mast cup anemometers at heights of 3 m, 15 m, 36 m, and 58 m. TurbSim version 2 [25] has the capability to match a wind time series in the *u*, *v*, and *w* axes, at a specified point in the rotor plane and extrapolate the full-field turbulence using spatial coherence models. To recreate field wind conditions, the nacelle wind measurement was used to match the simulation wind time series at hub height, whereas the sonic anemometer was used to create statistical probability distributions for the transverse wind speed components in the *v* and *w* directions. The wind measurements at different heights along the met mast were used to define the vertical shear. The synthetic full-field wind files were then used to run OpenFAST simulations with the SUMR-D model, and the results were compared as shown in figure 8. There was a good match between the simulations and the field tests across datasets, thus validating the simulation model as capturing most of the SUMR-D dynamics sufficiently well. The model validation has motivated further study, extension, and application of advanced control techniques [26] that can be assessed within similar simulations.

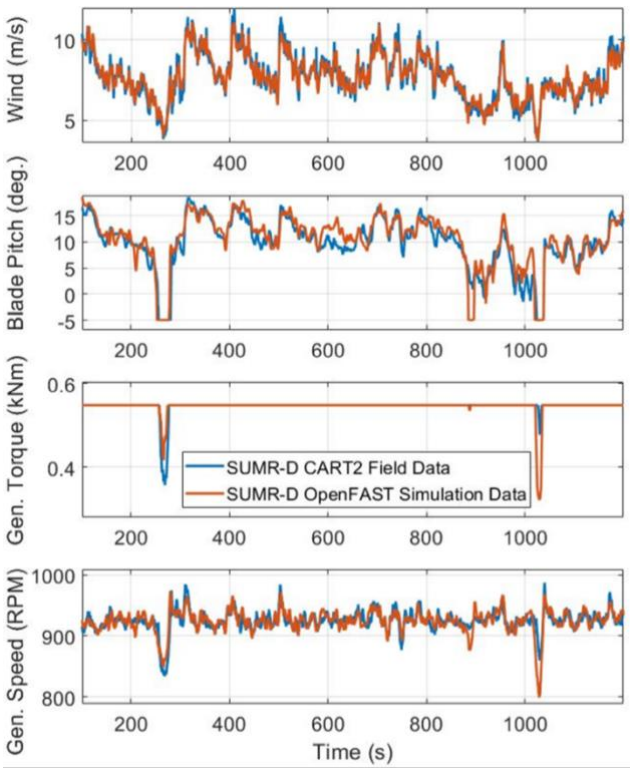

Figure 8. Control comparison of representative SUMR-D field data with OpenFAST simulations.

8. SUMR-D shutdown control performance

Based on the location at which the SUMR-D was installed having extreme wind conditions, the turbine's ability to survive a variety of shutdown cases was an important part of the design process. Therefore, in addition to validating the operational controller (Section 7), the ultimate blade root bending moment was examined in all of the field cases in which shutdowns occurred. These cases were characterized to correspond to the IEC design load cases (DLCs) for a fair comparison to the OpenFAST simulations. Figure 9 (data from Nov. 2, 2019, to Feb. 25, 2020) shows that field data loads for situations corresponding to DLC 5.1 are typically within the range predicted by OpenFAST, lending confidence to its use for shutdown control design.

A more detailed investigation was performed on one of the worst-case scenarios: a stuck blade case. Figure 10 shows the wind speed, blade pitch angle, and RootMxy (the vector sum of the blade root edgewise and flapwise bending moments) for this incident. This incident occurred near the rated wind speed (which is low due to gravo-aeroelastic scaling for this field test turbine). Both blades survived these loads and all other events, indicating successful controller shutdown performance.

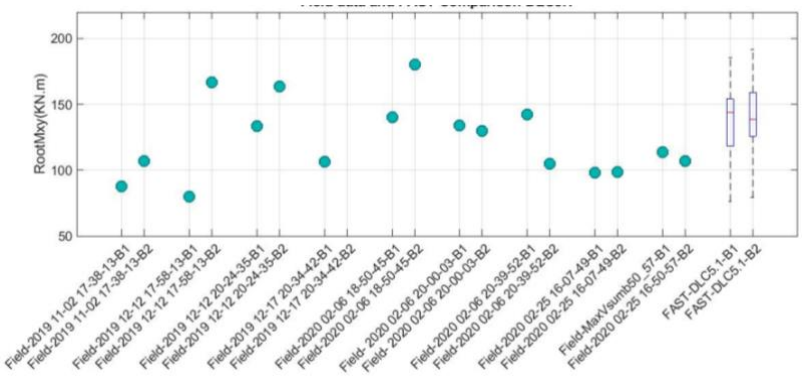

Figure 9. Comparison between the field and simulation data for root bending moment for field situations similar to DLC 5.1.

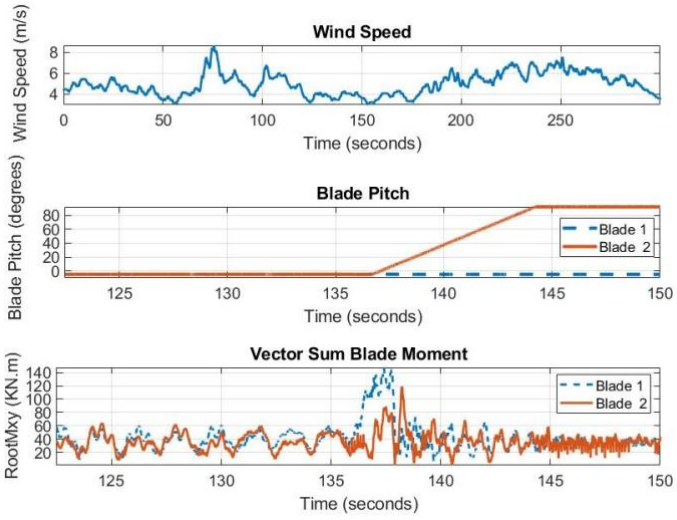

Figure 10. Rare event of a stuck blade failure (Blade 1), which has a higher max bending moment than Blade 2.

9. Blade loads and tower shadow

To investigate blade loading, the digital twin structural model and the above controllers were used in the OpenFAST simulations. Turbulent wind field files were built in TurbSim v2 to match meteorological tower data at the CART2 field site [27]. Blade root bending moment was the main response variable used to compare between simulations and experimental field test data. A key aspect of the SUMR concept is load alignment, whereby the rotor is designed so that the mean flapwise moments can be near zero for significant portions of the operation. However, there have been no operational measurements to confirm this load-alignment concept.

Figure 11 shows the bending moments as a function of wind speeds (normalized by the rated wind speed) for SUMR-D experiments. As predicted by FAST simulations for the configuration, these clearly

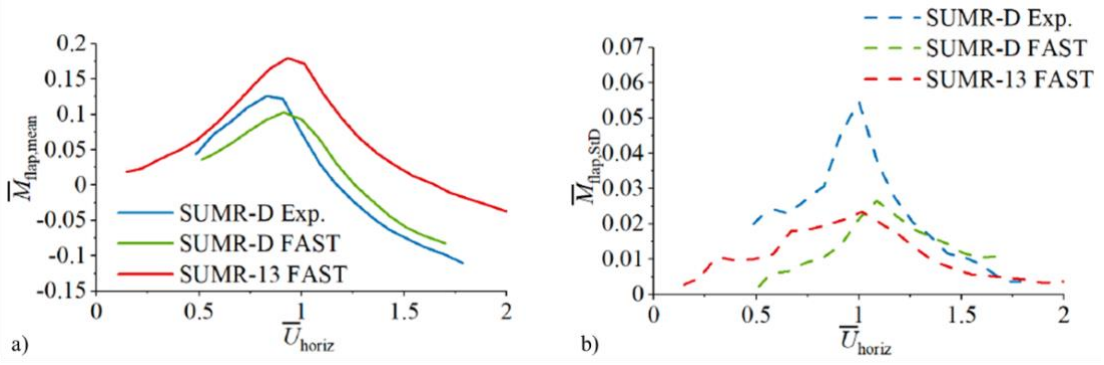

Figure 11. Experimental nondimensional flapwise bending moments vs. predictions for the digital twin of the SUMR-D and the SUMR-13 rotors showing a) the means and b) the standard deviations.

indicate load alignment at about 20% above rated conditions. The full-scale SUMR-13 was designed to achieve this load alignment at a higher wind speed, as shown by the FAST SUMR-13 simulations. These results demonstrate that the load alignment concept can be directly achieved during rotor operation with this downwind turbine.

Another issue is tower shadow. Downwind turbines experience the tower shadow effect when blades pass through the wake of the tower and experience a velocity deficit, resulting in reduced thrust loads and bending moments. To model tower shadow in OpenFAST, the aerodynamic subroutine AeroDyn15 [28] was used with the Powles tower shadow model [29]. Two example simulation results are compared to experimental data in figure 12. The tower shadow effect is more apparent in Region 3 (figure 12b) than in Region 2 (figure 12a), with a strong load reduction seen after the blade passes behind the tower (dotted vertical line). However, the net effect relative to turbulence is minimal. Thus, based on the results from this field test, tower shadow appears to have minimal impact on flapwise moments of flexible downwind rotors. Additional analysis, including fatigue, can be found in [30]. It is recommended that future downwind turbine designs include a tower shadow model to capture loading and fatigue effects on the rotor.

Finally, rotor noise was also evaluated with human observers (as close as testing constraints allowed) during field operation. The rotor was generally very quiet during operation with no evidence of rotor thump for this two-bladed downwind design. This was attributed to the combination of coning and aeroelasticity, which serves to provide good clearance and flexibility.

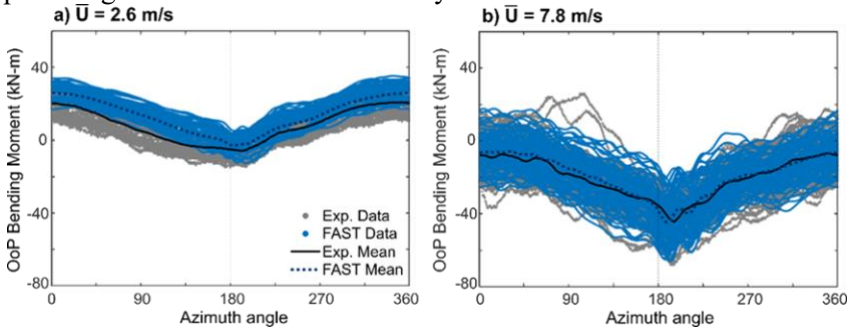

Figure 12. Blade 1 out-of-plane (OoP) bending moment data and azimuth-averaged mean for SUMR-D and OpenFAST for 5 minutes of operation for a) below-rated and b) above-rated wind speeds.

Conclusions

A highly flexible downwind load-aligned design was successfully designed and field tested at NREL's Flatirons Campus for a wide range of flow conditions. The turbine was designed with gravo-aeroelastic scaling to mimic the behavior of a 13-MW downwind turbine (the first ever such test). The tests demonstrated the benefits of a downwind rotor using load alignment, which may be beneficial at extreme scales (>10 MW). In particular, the experimental results confirmed two key advantages: 1) reduced flapwise moments and tower strike issues and 2) reduced rotor mass due to (1). The downwind load-aligned design concept also facilitates use of blade segmentation (as show by design and computational analysis) and the downwind orientation with shaft tilt can provide reduced wake losses for turbines.

The test also showed that four typical concerns for downwind turbines are not problematic:

1. Increased complexity associated with flexible lighter blades was handled in terms of design, computational predictions and was **not** a problem with operational or parked performance.
2. Increased noise in the form of a low frequency "thumping" noise was **not** observed.
3. Increased fatigue loads due to tower shadow were **not** seen (turbulence instead dominated).
4. Reduced power due to the reduced swept area can be avoided by adjusting coning angle.

Acknowledgments

This work was supported and funded in part by the Advanced Research Projects Agency – Energy (ARPA-E), U.S. Department of Energy, under Award Number DE-AR0000667.

This work was authored in part by the National Renewable Energy Laboratory, operated by Alliance for Sustainable Energy, LLC, for the U.S. Department of Energy (DOE) under Contract No. DE-AC36-08GO28308. Funding provided by U.S. Department of Energy Office of Energy Efficiency and Renewable Energy Wind Energy Technologies Office. The views expressed in the article do not necessarily represent the views of the DOE or the U.S. Government. The U.S. Government retains and the publisher, by accepting the article for publication, acknowledges that the U.S. Government retains a nonexclusive, paid-up, irrevocable, worldwide license to publish or reproduce the published form of this work, or allow others to do so, for U.S. Government purposes.

References

[1] Loth, E., Steele, A., Qin, C., Ichter, B., Selig, M. S., & Moriarty, P. (2017). Downwind pre-aligned rotors for extreme-scale wind turbines. *Wind Energy*, *20*(7), 1241-1259.

[2] Ichter, B., Steele, A., Loth, E., Moriarty, P., & Selig, M. (2016). A morphing downwind-aligned rotor concept based on a 13-MW wind turbine. *Wind Energy*, *19*(4), 625-637.

[3] Pao, L. Y., Zalkind, D. S., Griffith, D. T., Chetan, M., Selig, M. S., Ananda, G. K., ... & Loth, E. (2021). Control co-design of 13 MW downwind two-bladed rotors to achieve 25% reduction in levelized cost of wind energy. *Annual Reviews in Control, 51*, 331-343.

[4] Zalkind, D. S., Ananda, G. K., Chetan, M., Martin, D. P., Bay, C. J., Johnson, K. E., ... & Pao, L. Y. (2019). System-level design studies for large rotors. *Wind Energy Science*, *4*(4), 595-618.

[5] Qin, C., Loth, E., Zalkind, D. S., Pao, L. Y., Yao, S., Griffith, D. T., ... & Damiani, R. (2020). Downwind coning concept rotor for a 25 MW offshore wind turbine. *Renewable Energy*, *156*, 314-327.

[6] Kaminski, M., Loth, E., Zalkind, D., Pao, L., Selig, M., & Johnson, K. (2020). Servo-aero-gravo-elastic (SAGE) scaling and its application to a 13-MW downwind turbine. *Journal of Renewable and Sustainable Energy*, *12*(6), 063301.

[7] Yao, S., Griffith, D. T., Chetan, M., Bay, C. J., Damiani, R., Kaminski, M., & Loth, E. (2020). A gravo-aeroelastically scaled wind turbine rotor at field-prototype scale with strict structural requirements. *Renewable Energy*, *156*, 535-547.

[8] Kaminski, M., Loth, E., Griffith, D. T., & Qin, C. (2020). Ground testing of a 1% gravo-aeroelastically scaled additively-manufactured wind turbine blade with bio-inspired structural design. *Renewable Energy*, *148*, 639-650.

[9] Bay, C. J., Damiani, R., Fingersh, L. J., Hughes, S., Chetan, M., Yao, S., ... & Loth, E. (2019). Design and testing of a scaled demonstrator turbine at the National Wind Technology Center. In *AIAA Scitech 2019 Forum* (p. 1068).

[10] Yao, S., Griffith, D. T., Chetan, M., Bay, C. J., Damiani, R., Kaminski, M., & Loth, E. (2019). Structural design of a 1/5th scale gravo-aeroelastically scaled wind turbine demonstrator blade for field testing. In *AIAA Scitech 2019 Forum* (p. 1067).

[11] Selig, M. S., & Tangler, J. L. (1995). A multipoint inverse design method for horizontal axis wind turbines. *Wind Engineering*, 19, 91–105.

[12] Selig, M. (1995). PROPID–software for horizontal-axis wind turbine design and analysis. URL: http://www.ae.illinois.edu/m-selig/propid.html.

[13] Selig, M. S., & Maughmer, M. D. (1992). Generalized multipoint inverse airfoil design. *AIAA Journal*, *30*(11), 2618-2625.

[14] Selig, M. S. (1992). *Multi-point inverse design of isolated airfoils and airfoils in cascade in incompressible flow*. PhD Dissertation. The Pennsylvania State University.

[15] Drela, M., & Giles, M. B. (1987). Viscous-inviscid analysis of transonic and low Reynolds number airfoils. *AIAA Journal*, *25*(10), 1347-1355.

[16] Drela, M. (1989). XFOIL: An analysis and design system for low Reynolds number airfoils. In *Low Reynolds Number Aerodynamics* (pp. 1-12). Springer, Berlin, Heidelberg.

[17] Ananda, G. K., Bansal, S., & Selig, M. S. (2018). Aerodynamic design of the 13.2 MW SUMR-13i wind turbine rotor. *2018 AIAA SciTech Forum* (p. 0994).

[18] Jonkman, J. M., & Buhl Jr, M. L. (2005). FAST user's guide. *Golden, CO: National Renewable Energy Laboratory*, NREL/EL-500-38230, Golden, CO.
[19] Martin, D. P., Johnson, K. E., Zalkind, D. S., & Pao, L. Y. (2017). LPV-based torque control for an extreme-scale morphing wind turbine rotor. In *Proc. American Control Conference*, pp. 1383-1388.
[20] Zalkind, D. S., Pao, L. Y., Martin, D. P., & Johnson, K. E. (2017). Models used for the simulation and control of a segmented ultralight morphing rotor. *IFAC-PapersOnLine*, *50*(1), 4478-4483.
[21] International Electrotechnical Commission, *IEC 61400-1, Third Ed. 2005-2008. Wind Turbines – Part I: Design Requirements*, Standard, IEC, 2005.
[22] Griffith, D. T., & Richards, P. W. (2014). The SNL100-03 blade: design studies with flatback airfoils for the Sandia 100-meter blade. *SANDIA Report, SAND2014-18129*, *465*.
[23] Yao, S., Chetan, M., & Griffith, D. T. (2021). Structural design and optimization of a series of 13.2 MW downwind rotors. *Wind Engineering*, 0309524X20984164.
[24] Chetan, M., Yao, S., & Griffith, D. T. (2021). Multi-fidelity digital twin structural model for a sub-scale downwind wind turbine rotor blade. *Wind Energy*.
[25] Jonkman, B. J. (2009). *TurbSim user's guide: Version 1.50* (No. NREL/TP-500-46198). National Renewable Energy Lab.(NREL), Golden, CO (United States).
[26] Zalkind, D. S., Nicotra, M. M., & Pao, L. Y. (2021). Constrained power reference control for wind turbines. *Wind Energy*. DOI: 10.1002/we.2705.
[27] Simpson, J., & Loth, E. (2021). Field Tests and Simulations of Tower Shadow Effect for a Downwind Turbine. In *AIAA Scitech 2021 Forum* (p. 1718).
[28] Jonkman, J. M., Hayman, G. J., Jonkman, B. J., Damiani, R. R., & Murray, R. E. (2015). AeroDyn v15 user's guide and theory manual. *NREL Draft Report*.
[29] Powles, S. R. J. (1983). The effects of tower shadow on the dynamics of a horizontal-axis wind turbine. *Wind Engineering*, 26-42.
[30] Simpson, J. G., Kaminski, M., & Loth, E. (2021). Influence of tower shadow on downwind flexible rotors: Field tests and simulations. *Wind Energy*. DOI: 10.1002/we.2703.